# A computational study of the electronic structure and optical properties of the complex TeO 2 /TeO 3 oxides as advanced materials for nonlinear optics

E Roginskii, M Smirnov, V. Kuznetsov, O. Noguera, J. Cornette, Olivier Masson, Philippe Thomas

# A computational study of the electronic structure and optical properties of the complex $TeO_2/TeO_3$ oxides as advanced materials for nonlinear optics

**E M Roginskii[1], M B Smirnov[2], V G Kuznetsov[2], O Noguera[3], J Cornette[3], O Masson[3] and P Thomas[3]**

[1] Ioffe Institute, 194021 Polytekhnicheskaya 26, St. Petersburg, Russia

[2]Faculty of Physics St Petersburg State University, Petrodvoretz 194508, St Petersburg, Russia

[3]Institut de Recherche sur les Céramiques (IRCER)–UMR CNRS 7315, Université de Limoges, Centre Européen de la Céramique, 12 rue Atlantis, 87068 Limoges Cedex, France

**Abstract.** Electronic structure of series of tellurium oxide crystals within the $TeO_2$—$TeO_3$ binary system is studied with generalized gradient approximation to DFT, hybrid DFT-HF method with the PBE0 and B3LYP exchange-correlation functionals and with quasiparticle $G_0W_0$ approach. Comparison with available experimental data revealed significant underestimation of the band gap values within DFT. The hybrid DFT-HF method leads to slightly overestimated values of the bandgap, and the best agreement with experimental data provides the "one-shot" $G_0W_0$ calculations starting from Kohn-Sham solutions. The electronic structure of tellurium oxides is discussed in details. It is found that bandgap value decreases proportionally to fraction of tellurium atoms in octahedral coordination. This change is due to formation of gap states by 5s(Te) electrons which do not participate in Te(VI)–O bonding. Dielectric properties is calculated within Random Phase approximation for the series of tellurium oxides and high nonlinear properties of the compounds is predicted by empirical Miller's rule.

*Keywords*: *Ab initio*; DFT; GW; tellurium oxides; nonlinear optics; electronic structure

## 1. Introduction

Tellurium dioxide $TeO_2$ in crystalline and glassy state attracts considerable attention as a material with outstanding non-linear optical (NLO) properties. The third-order non-linear refractive index of glassy $TeO_2$ is 50 times higher than that of the silica glass [1]. The $\alpha$-$TeO_2$ exhibits also outstanding optoacoustic, piezoelectric and electro-optic properties [3, 4]. The crystalline modification $\gamma$-$TeO_2$ gives evidence of a strong second-harmonic generation effect [2]. Moreover, recently it was revealed that another crystalline tellurium oxide $Te_2O_5$ possess the extremely high second harmonic generation coefficient two order higher than quartz [5].These findings gave rise to a large body of researches aimed to search of advanced NLO materials via doping the $TeO_2$ by different modifiers with highly polarizable cations [6]. In spite of great number of such investigations, they gave quite inferior success.

However, there is another approach related to alteration of the oxidation state of the tellurium atoms. The Te atoms are polyvalent – depending on chemical environment they may take the Te(IV) or Te(VI) oxidation state. This gives rise to existence of several stable oxides with chemical formula $Te_4O_x$ ($8 < x < 12$) which can be considered as mixed $TeO_2$/$TeO_3$ compounds. The NLO properties of the mixed tellurium oxides are not yet studied experimentally, but preliminary theoretical estimations [7] predicted an enhancement of the third-order hyperpolarizability along with the increase of $TeO_3$ content. This effect was associated with variation of the electronic bandgap. Indeed, the experimental optical absorption measurements and theoretical estimations agreed that the bandgap is twice narrower in $TeO_3$ than in $TeO_2$ [8]. At the same time, the rather accurate quantum-mechanical calculations predicted for $TeO_3$ the NLO susceptibility twice as less than for $TeO_2$. The result seems quite paradoxical. Usually the polarizability (and hyperpolarizability) is in inverse dependence of the bandgap value [9, 10]. Violation of the universal relationship in the case of $TeO_2$ and $TeO_3$ compounds was associated with peculiarities of the electronic structures, namely with the so the called lone-pairs – specific electron states which exist in $TeO_2$ and are absent in $TeO_3$. This feature opens up possibility to synthesize the compounds with chemical formula $Te_4O_x$ with variable bandgap and polarizability (hyperpolarizability) values by changing the Te(IV)/Te(VI) ratio. Such possibility would exists if the both quantities vary monotonously along with $x$ variation. The present paper is aimed to study the variation of the electronic structure and dielectric susceptibility of a series of tellurium oxides $Te_4O_x$ ($8 < x < 12$). The study is based on the quantum-mechanical simulations with the use of the thoroughly chosen *ab initio* method.

## 2. Computational details

The density functional calculations presented in the paper were carried out within generalized gradient approximation (GGA) to DFT with exchange-correlation PBEsol functional [11] using the pseudopotential method and the plane-wave basis set for valence electronic states as implemented in ABINIT software package [12,13]. The 4d5s5p states of Te atom and 2s2p states of O atom were considered as valence states.

For each system the atomic positions and lattice parameters have been optimized via independent relaxation until the atomic forces and stresses were reduced below $10^{-5}$ Ha/Bohr and 0.2 Kbar, respectively. The results were checked for the convergence with respect to the size of k-point sampling integration grid and to the plane-wave kinetic energy cutoff. It was found that the convergence of total energy within 0.1 mHa was achieved with the energy cutoff of 40 Ha. The k-point grids were chosen according to the Monkhorst-Pack scheme [14] as $6 \times 6 \times 4$ for $\alpha$-$TeO_2$ and $Te_2O_5$, $6 \times 6 \times 6$ for $\beta$-$TeO_3$ and $5 \times 5 \times 5$ for $Te_4O_9$ crystals in the DFT calculations. The $4 \times 4 \times 4$

Monkhorst-Pack grid for all studied compounds was found to be acceptable for the hybrid PBE0 functional [15] and quasiparticle $GW$ calculations [16] with convergence of total energy equal to 0.05 eV. Since hybrid functional and $GW$ methods are high resource demanding, the electronic structure was calculated by these methods using structural parameters obtained with PBEsol functional approximation calculations.

The one-shot $G_0W_0$ quasiparticle energies were computed using Kohn-Sham eigenstates and eigenvalues as an initial solution of non-interacting Hamiltonian. The inverse dielectric matrix $\epsilon^{-1}_{GG'}(\mathbf{q},\omega)$ was calculated by random phase approximation (RPA) using 250 unoccupied bands. Dynamic screening was calculated using contour deformation method [17]. The wavefunctions with maximal kinetic energy 35 Ha were used in the calculations. The corrections to Kohn-Sham energies were calculated as $[\Sigma - E_{xc}]$ operator diagonal matrix elements, where $\Sigma = GW$ — self-energy operator, $E_{xc}$ — exchange-correlation energy operator, $G$ — Green function, and $W = \epsilon^{-1}v$ — screening Coulomb interaction operator. The components of wavefunction with energies below 35 Ha for both exchange and correlation part were used to calculate $\Sigma$.

The $GW$ electronic band structure and density of states was obtained by correction of the Kohn-Sham ones by applying energy-dependent scissors operator generated by fitting $GW$-KS energy differences over dense grid of $k$-points as a function of the KS eigenvalues.

The calculations within density functional theory realized in Beck's three-parameter hybrid method using the Lee-Yang-Parr correlation functional (B3LYP) [18,19] was also performed by using CRYSTAL14 software package [20]. This method was implemented with the localized atomic functions (LCAO) basis set, namely 311G* for Te and 3-21G for O atom [21,22].

## 3. Results and Discussion

### *3.1. Crystal structure*

We consider four crystalline tellurium oxides, namely $TeO_2$, $Te_4O_9$, $Te_2O_5$, and $TeO_3$. They can be represented as the members of the series (1-$\kappa$) $TeO_2$ + $\kappa$ $TeO_3$ with $\kappa$ = 0, 0.25, 0.5, 1. All these crystals were synthesized and characterized by using different experimental techniques (see [23] for references). The crystal structures are plotted in Figure 1. One can see that in these structures the Te atoms are surrounded either by six O atoms, or by four O atoms. Fraction of the formers just corresponds to the $\kappa$ value.

The structure with $\kappa$=0 is the tellurium dioxide $\alpha$-$TeO_2$ (paratellurite). The lattice is 3D framework built of the corner-sharing disphenoids $TeO_4$. The structure with $\kappa$=1 is the tellurium trioxide $\beta$-$TeO_3$. The lattice is 3D framework built of the corner-sharing octahedra $TeO_6$. The structural units of $\alpha$-$TeO_2$ ($\kappa$=1) crystal are $TeO_4$ disphenoids with two short equatorial Te-$O_{eq}$ and two longer axial Te-$O_{ax}$ bonds [24]. In the structures of mixed tellurium oxides $Te_4O_9$ and $Te_2O_5$ there are corner-sharing disphenoids and octahedra presented in the ratio $(1-\kappa)/\kappa$. The $Te_2O_5$ structure is a

3D framework, and the $Te_4O_9$ structure has a layered constitution with large interlayer separation. According to oxidation state, we shall refer the tellurium atoms in the center of $TeO_6$ octahedra and the $TeO_4$ disphenoids as Te(VI) and Te(IV). The first stage of the study involved search of the *ab initio* approach which assures reliable reproduction of the experimental crystal structures. Methods used in the preceding studies [7, 25] markedly overestimated the unit cell dimensions (see Table 1). The PBEsol functional approximation used in this study provides a very good agreement with experimental data. Calculated atomic positions and bond lengths also agree well with the experimental data. These results with respect to experimental data are reported in Tables S1-S5 of the Supplementary Material.

The symmetry of $\alpha$-$TeO_2$ crystal is $P4_12_12$ and, as mentioned above, the structural units are $TeO_4$ disphenoids with two short equatorial Te-$O_{eq}$ and two longer axial Te-$O_{ax}$ bonds [24] thus tellurium atoms in the crystal are expected to be in Te(IV) valence state. The symmetry of $\beta$-$TeO_3$ is $R\bar{3}c$ and the $TeO_6$ octahedra are found to be the structural unit of the crystal [26] thus the tellurium atoms are expected to be in Te(VI) valence state. The combination of different portions of Te(IV) and Te(VI) fractions lead to formation of complex $Te_4O_9$ and $Te_2O_5$ tellurium oxides with $R\bar{3}$ and $P2_1$ space group symmetry correspondingly.

### *3.2. Electronic band structure*

Second stage consisted in the electron band structure simulation. The bandgap values calculated by different DFT methods are listed in Table 2 in comparison with available experimental data and previous computational studies. One can see the significant underestimation of the bandgap values in case of DFT without non-local exchange term. Unfortunately, experimental estimations of the bandgap values are known only for $\alpha$-$TeO_2$ and $\beta$-$TeO_3$. The highest disagreement with experiment (error more than 60%) occurs for the $\beta$-$TeO_3$ studied with PBEsol functional. Hence, this approximation could not predict optical properties (which strongly depend on electronic structure) with reasonable accuracy. In contrast, addition of the exact Hartree-Fock term within the B3LYP approximation leads to overestimation of the bandgap value by approximately 10% in case of $\alpha$-$TeO_2$. The best agreement with experimental data was found for the self-consistent $GW$ approximation [8], but this type of computations is very expensive. The results presented in Table 2 show that the “single-shot” $G_0W_0$ approximation, which is less time-consuming, also predicts the value of the band gap in a good agreement with experimental data.

The electronic band structures calculated within quasiparticle $G_0W_0$ approximation for the series of tellurium oxides are plotted in Figure 2. As mentioned above the values of indirect bandgap for $\alpha$-$TeO_2$ and $\beta$-$TeO_3$ are in a good agreement with experimental data.

Analysis of the Figure 2 shows that the only compound with direct optical transition is $\beta$-$TeO_3$. For $\alpha$-$TeO_2$ oxide the minimum of the conduction band ($E_c^{min}$) is located

**Table 1.** Unit cell parameters $a$,$b$,$c$ (in Å) and specific volume $V_0$ (per formula unit, in Å$^3$) for the $Te_4O_x$ crystals calculated by hybrid-functional B3LYP (CRYSTAL) method, and by generalized gradient approximation to DFT using PBEsol functional (ABINIT) compared with experimental data and previously reported calculations (SIESTA).

| x | | Exp.* | PBE [7] | B3LYP** | PBEsol |
|---|---|---|---|---|---|
| 8 | $a = b$ | 4.808 | 4.987 | 4.899 | 4.840 |
| | $c$ | 7.612 | 7.606 | 7.777 | 7.434 |
| | $V_0$ | 43.991 | 47.129 | 46.662 | 43.526 |
| 9 | $a = b$ | 9.32 | 9.589 | 9.491 | 9.373 |
| | $c$ | 14.486 | 15.032 | 15.091 | 14.593 |
| | $V_0$ | 45.405 | 49.875 | 49.052 | 46.264 |
| 10 | $a$ | 5.368 | 5.598 | 5.477 | 5.496 |
| | $b$ | 4.696 | 4.805 | 4.771 | 4.724 |
| | $c$ | 7.955 | 8.160 | 8.094 | 8.001 |
| | $\beta\circ$ | 104.82 | 102.94 | 104.82 | 102.86 |
| | $V_0$ | 48.465 | 53.479 | 51.117 | 50.63 |
| 12 | $a = b$ | 4.901 | 5.055 | 5.004 | 4.979 |
| | $c$ | 13.030 | 13.447 | 13.224 | 13.198 |
| | $V_0$ | 45.174 | 49.596 | 47.794 | 47.221 |

*Experimental data from Ref. [24, 26–28]
**Data for $TeO_2$ and $TeO_3$ are taken from Ref. [25]

**Table 2.** Calculated by different approximations band gap values of $Te_4O_x$ crystals (in units of eV) in comparison with experimental data.

| x | Experimental [8, 29] | $GW$ [8] | LDA+$U$ [8] | PBEsol | PBE0 | B3LYP | $G_0W_0$ |
|---|---|---|---|---|---|---|---|
| 8 | 3.75 | 3.68 | 3.26 | 2.80 | 4.48 | 4.26 | 3.56 |
| 9 | - | - | - | 2.11 | 3.82 | 3.95 | 3.50 |
| 10 | - | - | - | 1.71 | 3.44 | 3.57 | 3.13 |
| 12 | 3.25 | 2.74 | 2.27 | 1.21 | 3.16 | 3.41 | 2.52 |

in the vicinity of $X$-point, namely at the (0,1/6,0) point of the Brillouin zone (BZ), the maximum of valence zone ($E_v^{max}$) is located at the (1/4,1/4,0) point of the BZ. In the case of $Te_4O_9$ the $E_c^{min}$ is located at $T$-point (1/2,1/2,1/2) and $E_v^{max}$ is found at F-point (1/2,1/2,0) of the BZ. Finally for $Te_2O_5$ the minimum of conducting band is located at $B$-point (0,0,1/2) and maximum of the valence band at $Y$ point (1/2,0,0) of the BZ. In the latter case the difference between values of the direct bandgap at $\Gamma$-point ($E_g^d(\Gamma)$) and indirect bandgap ($E_g^i$) is less than 0.2 eV, while for $\alpha$-$TeO_2$ and $Te_4O_9$ the difference is more than 1 eV. The band structures shown in Figure 2 markedly differ in the bottom part of the conduction band. Dispersion of the bands, their number

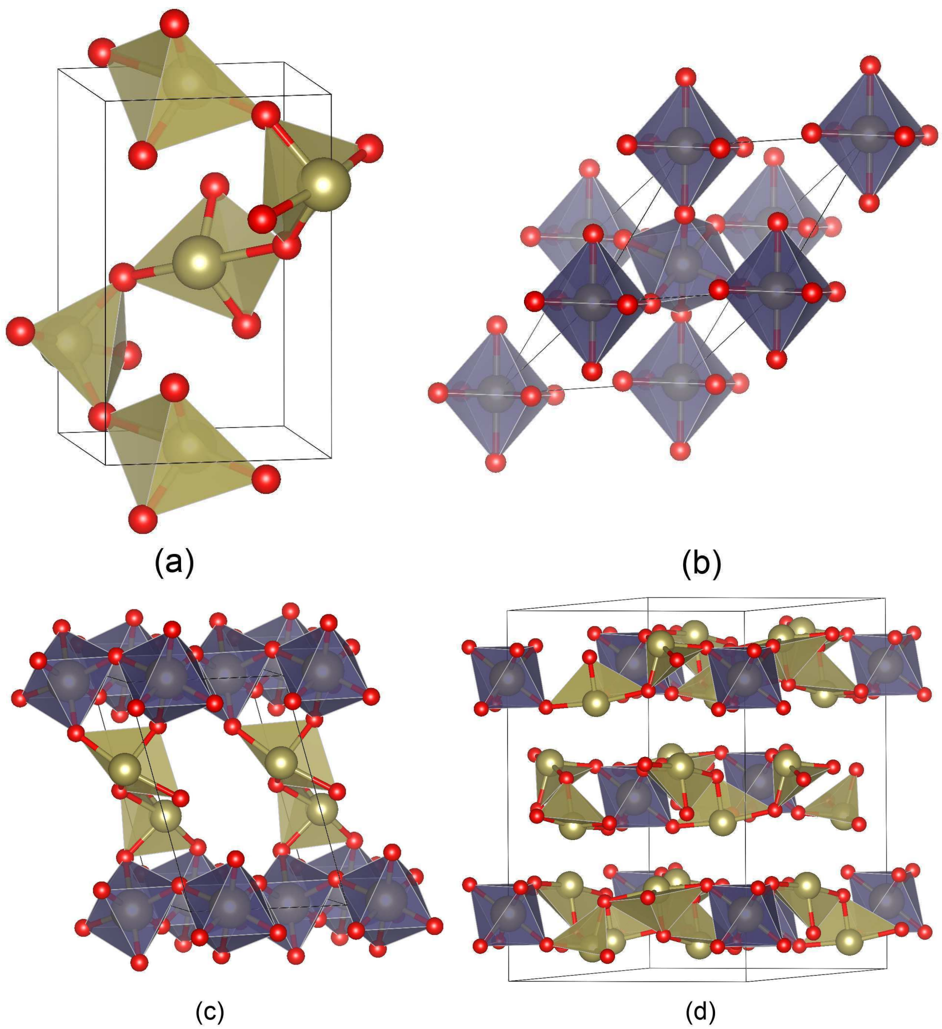


**Figure 1.** Crystal structures of $\alpha$-$TeO_2$ (a) $\beta$-$TeO_3$ (b) $Te_2O_5$ (c) and $Te_4O_9$ (d)

and density depend on the size of the unit cell and on the structural composition (concentration of disphenoids and octahedra) as well. A more detailed understanding could be derived from analysis of the partial density of states of these crystals.

The calculated partial Density of State (DOS) functions decomposed into Te and O contributions are plotted in Figure 3. One can see that the O and Te contributions are markedly mixed in the states below -3 eV. These electron states are responsible for formation of the Te-O valence bonds. This part of the DOS is divided in two features centered around -9 and -5 eV. They correspond to the bonding and antibonding combinations of the Te-O orbitals respectively. Besides, both the bonding and antibonding DOS features are twice split in $\alpha$-$TeO_2$. This splitting is due to non-equivalence of the axial and equatorial bonds in the disphenoids. Such splitting is absent in $\beta$-$TeO_3$ because the Te-O-Te bridges are symmetric. The complex oxides $Te_4O_9$ and $Te_2O_5$ exhibit peculiarities of both $\alpha$-$TeO_2$ and $\beta$-$TeO_3$ since they are constructed from octahedra and disphenoids general units, but more sharp splitting is found in DOS of

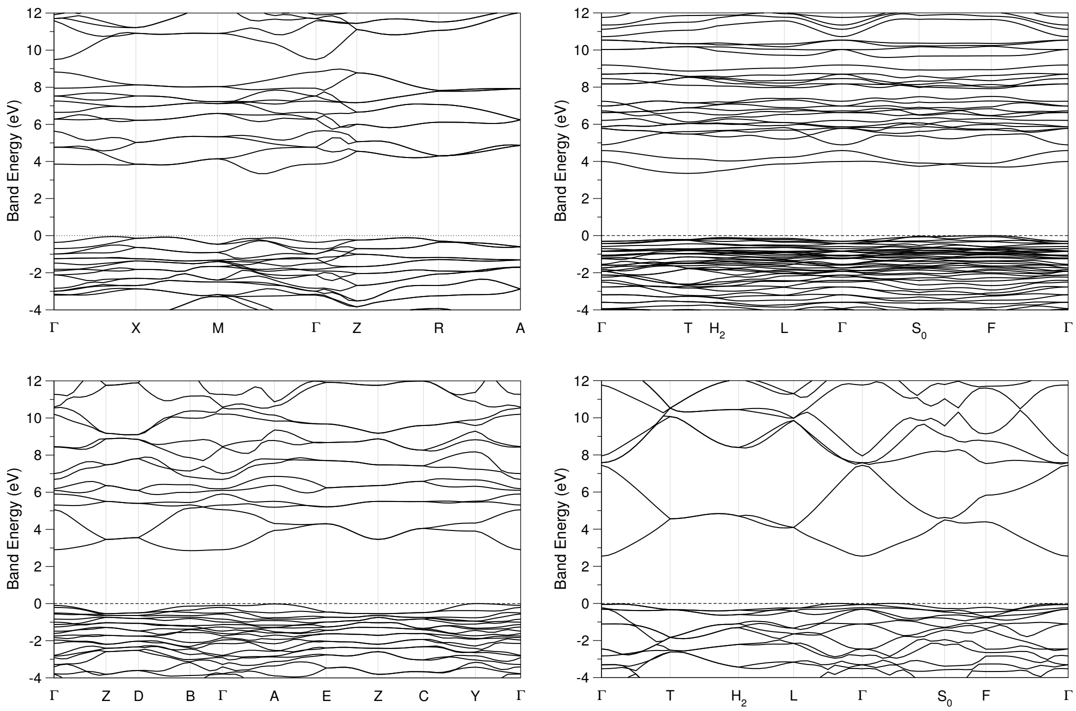


**Figure 2.** Electronic bandstructures (from top to bottom) of $\alpha$-$TeO_2$, $Te_4O_9$, $Te_2O_5$, and $\beta$-$TeO_3$

$Te_4O_9$ since the concentration of disphenoids is 3 times larger then in $Te_2O_5$.

Now we turn to the upper part of the valence band (UVB) and the bottom part of the conduction band (BCB). Namely these electron states play a key role in the polarization excitation process. One can see that the states in valence band above -3 eV consist predominantly of the O contributions. They correspond to the lone pairs (LP) localized on the oxygen atoms.‡ Meanwhile the Te contributions are quite noticeable in $\alpha$-$TeO_2$ and almost imperceptible in $\beta$-$TeO_3$. The situation is intermediate in the mixed $TeO_2/TeO_3$ oxides (see Figure 3c and 3d). It was shown before [8] that the difference between compositions of UVB and BCB states in $\alpha$-$TeO_2$ and $\beta$-$TeO_3$ was attributed to the tellurium lone pairs which exist in $\alpha$-$TeO_2$ and are absent in $\beta$-$TeO_3$. Now, it is appropriate to test if this idea can explain the electronic structure of the mixed tellurium oxides.

The LP(Te) states predominantly consist of the 5s(Te) contributions. It is worth to recall that complex oxides are composed by $TeO_4$ disphenoids and $TeO_6$ octahedra structural units. Thus, there are two types of tellurium atoms with different environment, namely, the tellurium atoms in disphenoids with four oxygen neighbour atoms (Te(IV)) and the other one in octahedras with six neighbour oxygen (Te(VI)). Hence, occupancies of the 5s(Te) states must differ markedly for the Te(VI) and Te(IV) atoms. Partial DOS functions decomposed into contributions of the 5s(Te) and 5p(Te)

‡ More detailed analysis shows that generally 2p(O) electrons contribute to these states. The electron levels corresponding to the 2s(O) electrons lay much lower at around -12 eV

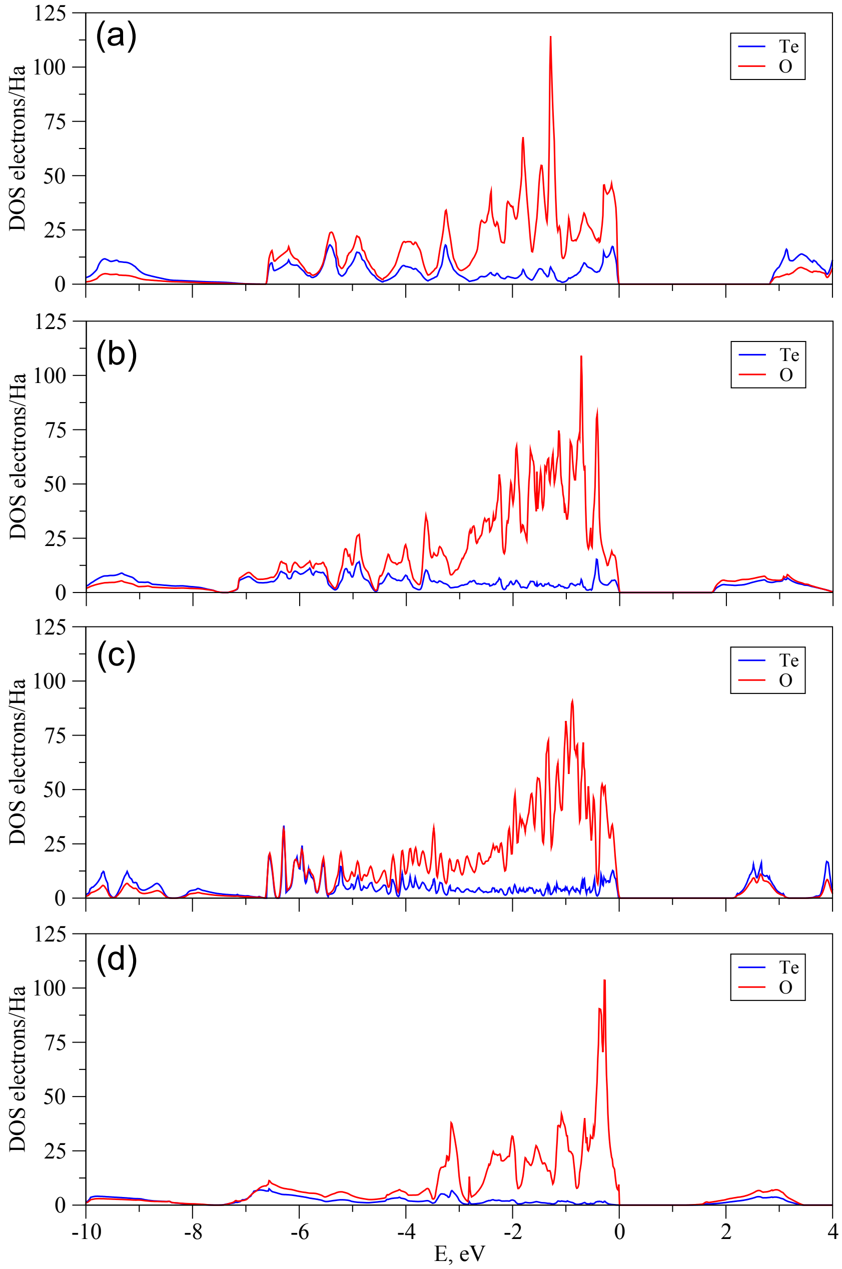


**Figure 3.** The partial density of states per one formula unit for $\alpha$-$TeO_2$ (a), $Te_4O_9$ (b), $Te_2O_5$ (c), and $\beta$-$TeO_3$ (d) calculated with PBEsol functional. The oxygen and tellurium DOS contribution are the local density of states calculated inside the sphere centered on atom with radius 1.24 Å and 0.63 Å for Te and O atoms correspondingly.

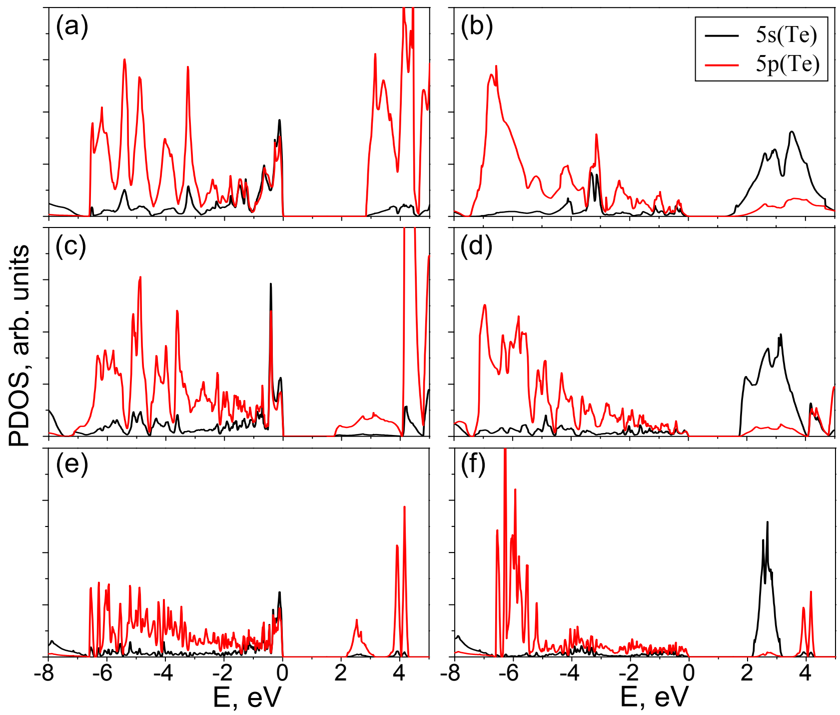


**Figure 4.** The partial DOS (PDOS) for Te(IV) and Te(VI) atoms in tellurium oxides calculated with PBEsol functional. (a) – PDOS for Te(IV) $\alpha$-$TeO_2$, (b) – PDOS for Te(VI) in $\beta$-$TeO_3$, (c,e) – PDOS for Te (IV) atoms in $Te_2O_5$ and $Te_4O_9$ correspondingly, and (d,f) – PDOS for Te (VI) atoms in $Te_2O_5$ and $Te_4O_9$ correspondingly. The partial DOS calculated inside the sphere centered on atom with radius 1.24 Å and 0.63 Å for Te and O atoms correspondingly.

states in vicinities of the UVB and BCB levels are shown in Figure 4. In all compounds there are two main differences between partial DOS calculated for the Te(IV) and Te(VI) atoms:

- 5s(Te(IV)) electrons contribute markedly to the UVB states and give nothing to the BCB states;
- 5s(Te(VI)) electrons do not contribute to the UVB states and form a strong sub-band in vicinity of BCB level.

The partial DOS shown in Figure 4 evidence that the 5s(Te(IV)) electrons participate significantly to the UVB states whereas the 5s(Te(VI)) contributions are markedly lesser in the valence band states. This difference results in total atomic occupancy which is about 10% larger for the Te(IV) atoms than for the Te(VI) atoms. It is remarkable that the occupancies are almost constant in all compounds. Thus one can suggest that Te(VI)–O bonds are by 10% more ionic than the Te(IV)–O bonds.

Summarizing, one can say that the 5s(Te) electron states of Te(IV) atoms migrate from the top of valence band to the bottom of the conduction band when the Te(IV) atom changes the oxidation state. Such DOS transformation results in two important changes:

- bandgap value decreases proportionally to concentration of the Te(VI) atoms;
- polarizability value may decrease in spite of the bandgap decrease.

The latter issue is caused by nonpolar nature of the 5s states [8]. To validate these statements within all the series, the additional calculations is required and the question will be studied in the forthcoming paper.

As mentioned above the main structural distinction between the $TeO_2$ and $TeO_3$ compounds concerns the Te-O-Te bridges. They are asymmetric (with equatorial and axial Te-O bonds) in $TeO_2$ and symmetric in $TeO_3$. This structural peculiarity manifests itself in the DOS distribution as the well pronounced splitting of the DOS features at around -9 and -5 eV. It can be suggested that the electronic states in the mixed $TeO_2$–$TeO_3$ oxides must correspond to the structural units typical for the both pure oxides. Moreover, we may suggest that these electron states contribute to the total DOS proportionally to their occurrences. To tests this hypothesis we have compared the electron DOS calculated for the $Te_4O_9$ and $Te_2O_5$ with the DOS combinations 3[$TeO_2$] + [$TeO_3$] and [$TeO_2$] + [$TeO_3$]. The results are shown in Figure 5.

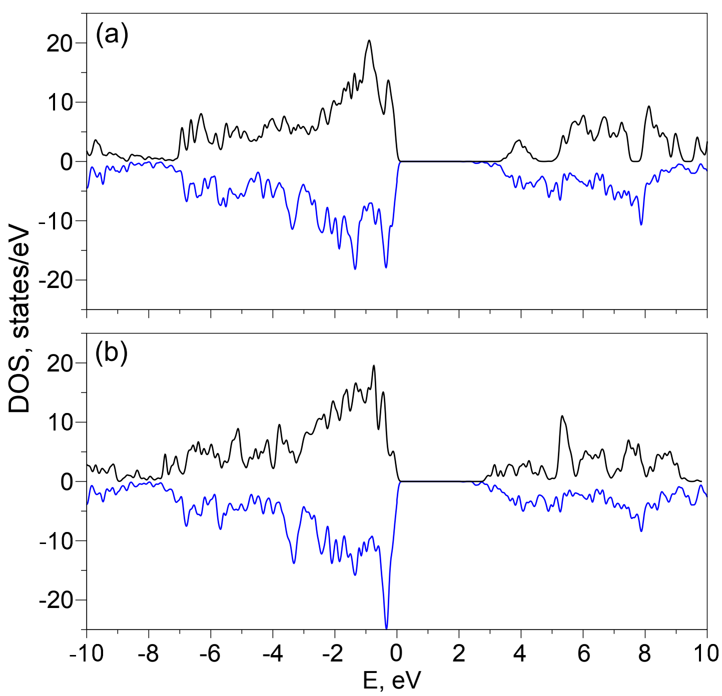


**Figure 5.** Calculated with $G_0W_0$ approximation electron DOS for the $Te_4O_9$ (a) and $Te_2O_5$ (b) crystals (black lines) compared with the DOS combinations 3[$TeO_2$] + [$TeO_3$] (a) and [$TeO_2$] + [$TeO_3$] (b) (blue lines). The DOS for $Te_2O_5$ are normalized by a factor of x2 to align the number of Te atoms in both compounds. The combined DOS functions were negated for the sake of clarity.

It is seen that properly combined DOS's of the pure $\alpha$-$TeO_2$ and $\beta$-$TeO_3$ oxides mimic quite correctly the DOS of the mixed $TeO_2/TeO_3$ compounds. The results presented in Figure 3 and Figure 5 allow us to make some remarks concerning the DOS variations in the $TeO_2$-$Te_4O_9$-$Te_2O_5$-$TeO_3$ series. An increase of the fraction of the symmetric Te-O-Te bridges results in gradual decrease of splitting in the DOS features around -9 and -5 eV. The progressive increase of the fraction of the Te (VI) atoms leads to formation of the smooth and wide DOS feature at the bottom of the conduction band. This feature is formed by 5s(Te) electron states which are empty in the Te(VI) atoms and contribute to BCB proportionally to the fraction of $TeO_6$ octahedrons.

### *3.3. Dielectric susceptibility*

Finally, it is noteworthy that the accurate electronic structure calculations leads to accurate prediction of dielectric properties. According to empiric Miller's rule a very simple relation was proposed in Ref [30]:

$$\chi^{(3)} \sim \left[\chi^{(1)}\right]^4 . \tag{1}$$

For isomorphic compounds the coefficient of the proportionality is expected to be nearly the same. Hence, one can roughly estimate the ratio of the third order susceptibilities using the calculated linear susceptibilities for simple and mixed oxides:

$$\frac{\chi^{(3)}(Te_4O_x)}{\chi^{(3)}(Te_4O_y)} \approx \left[\frac{\chi^{(1)}(Te_4O_x)}{\chi^{(1)}(Te_4O_y)}\right]^4 . \tag{2}$$

The linear susceptibilities were calculated within Random Phase Approximation [31, 32] using Green's functions $G$ and self energy operator $\Sigma$ calculated by $G_0W_0$ approximation. The mean values of linear susceptibility is reported in table **??**. It noteworthy, that the calculated value of $\chi^{(1)}$ for $TeO_2$ crystal is very close to the experimental one which is equal to 4.1 [33].

The linear susceptibilities were calculated within Random Phase Approximation [31, 32] using Green's functions $G$ and self energy operator $G$ calculated by $G_0W_0$ approximation. The mean values of linear susceptibility for the set of tellurium oxides was found to be equal to $\chi^{(1)}(TeO_2) = 3.91$, $\chi^{(1)}(Te_4O_9) = 3.2$, and $\chi^{(1)}(Te_2O_5) = 2.8$. The value of $\chi^{(1)}$ for $TeO_2$ crystal is very close to the experimental one which is equal to 4.1 [33]. Hence the calculation method of dielectric properties results is quite credible. The only known experimental value of the third order nonlinear susceptibility is for paratellurite crystal and the one is equal to $\chi^{(3)}(TeO_2) = 95.1 \times 10^{-22} m^2V^{-2}$ [34]. The value could be used as a reference and now applying equation 2 it is follows that the mean values for the nonlinear susceptibilities of mixed oxides are $\chi^{(3)}(Te_4O_9) \sim 40 \times 10^{-22}\ m^2V^{-2}$, and $\chi^{(3)}(Te_2O_5) \sim 24 \times 10^{-22}\ m^2V^{-2}$.

## 4. Conclusion

The close connection between crystal and electronic structures of the mixed $TeO_2/TeO_3$ compounds is revealed by analyzing the DOS distributions. It is shown that properly combined DOS's of the pure $TeO_2$ and $TeO_3$ oxides mimic rather well the DOS of the mixed crystals. Crystal structures of the mixed $TeO_2/TeO_3$ oxides contain two types of coordination polyhedra – the $TeO_4$ disphenoids and the $TeO_6$ octahedra. The tellurium atoms located within disphenoids and within octahedra are in the Te(IV) and Te(VI) oxidation states respectively. Coexistence of the disphenoids and octahedra (the Te(IV) and Te(VI) atoms) results in some peculiarities of the electronic structure.

The main peculiarity concerns the Te atom contributions to the upper part of the valence band and the bottom part of the conduction band. The former is proportional to the fraction of the Te(IV) atoms and the latter is proportional to the fraction of the Te(VI) atoms. This peculiarity can be attributed to the tellurium atom lone-pairs which exist in Te(IV) atoms and are absent in Te(VI) atoms. In case of e Te(IV) atoms, the existence of electron lone-pairs gives rise to a considerable contribution of the 5s(Te) electrons to the upper part of the valence band. When the Te(IV) atom oxidizes to the Te(VI) state, its lone pair transforms into two additional Te-O bonds, losses the 5s(Te) contribution, and markedly lowers in energy. The unoccupied 5s(Te) electron states migrate from the top of valence band to the bottom of the conduction band. Such DOS transformation results in variation of the bandgap value which decreases proportionally to concentration of the Te(VI) atoms. It is noteworthy that the bandgap narrowing does not result in the polarizability increase because of nonpolar character of the 5s(Te) states. The compounds considered in the study represent a rare example of violation of the universal law which states that polarizability is in inverse dependence of the bandgap value.

By using results of the dielectric properties calculations and empiric Miller's rule the third order nonlinear properties were predicted for all studied compounds, which is more than ten times higher than the one in silica glass widely used in technical application. Thus these compounds are very promising in technical application.

## 5. Acknowledgements

The authors acknowledge the financial support from the Russian Foundation for Basic Research (RFBR) № 18-03-00750. V. G. Kuznetsov also gratefully acknowledges support from the RBFR № 18-03-01220. The computations were performed using facilities of the Computational Centre of the Research Park of St. Petersburg State University.

## 6. ORCID iDs

E Roginskii https://orcid.org/0000-0002-5627-5877 M Smirnov https://orcid.org/0000-0002-4292-1989 V Kuznetsov https://orcid.org/0000-0003-1996-0055 O Noguera https://orcid.org/0000-0003-1021-1752 P Thomas https://orcid.org/0000-0002-8431-8272

## 7. References

[1] Kim S H, Yoko T and Sakka S 1993 *J. Am. Ceram. Soc.* **76** 2486–2490

[2] Vrillet G, Lasbrugnas C, Thomas P, Masson O, Couderc V, Barthélémy A and Champarnaud-Mesjard J C 2006 *J. Mater. Sci.* **41** 305–307
[3] Arlt G and Schweppe H 1968 *Solid State Commun.* **6** 783–784
[4] Ohmachi Y and Uchida N 1970 *J. Appl. Phys.* **41** 2307–2311
[5] Kong F, Sun C F, Yang B P and Mao J G 2012 Second-order nonlinear optical materials based on metal iodates, selenites, and tellurites *Structure-Property Relationships in Non-Linear Optical Crystals I* (Springer Berlin Heidelberg) pp 43–103
[6] El-Mallawany R 2012 *Tellurite Glasses Handbook: Physical Properties and Data, second ed.* (CRC Press)
[7] Plat A, Cornette J, Colas M, Mirgorodsky A, Smirnov M, Noguera O, Masson O and Thomas P 2014 *J. Alloys Compd.* **587** 120–125
[8] Roginskii E M, Kuznetsov V G, Smirnov M B, Noguera O, Duclère J R, Colas M, Masson O and Thomas P 2017 *J. Phys. Chem. C* **121** 12365–12374
[9] Moss T S 1985 *physica status solidi (b)* **131** 415–427
[10] Sheik-Bahae M, Hagan D J and Stryland E W V 1990 *Physical Review Letters* **65** 96–99
[11] Perdew J P, Ruzsinszky A, Csonka G I *et al.* 2008 *Phys. Rev. Lett.* **100** 136406
[12] Gonze X, Amadon B, Anglade P M *et al.* 2009 *Comput. Phys. Commun.* **180** 2582–2615
[13] Gonze X, Rignanese G, Verstraete M *et al.* 2005 *Z. Kristallogr. - Cryst. Mater.* **220** 558–562
[14] Monkhorst H J and Pack J D 1976 *Phys. Rev. B* **13** 5188–5192
[15] Perdew J P, Ernzerhof M and Burke K 1996 *J. Chem. Phys.* **105** 9982–9985
[16] Aulbur W G, Jnsson L and Wilkins J W 2000 Quasiparticle calculations in solids *Solid State Phys.* vol 54 (Elsevier BV) pp 1–218
[17] Lebègue S, Arnaud B, Alouani M and Bloechl P E 2003 *Phys. Rev. B: Condens. Matter Mater. Phys.* **67** 155208
[18] Vosko S H, Wilk L and Nusair M 1980 *Can. J. Phys.* **58** 1200–1211
[19] Becke A D 1993 *J. Chem. Phys.* **98** 1372–1377
[20] Dovesi R, Orlando R, Erba A, Zicovich-Wilson C M, Civalleri B, Casassa S, Maschio L, Ferrabone M, Pierre M D L, D'Arco P, Noël Y, Causà M, Rérat M and Kirtman B 2014 *Int. J. Quantum Chem.* **114** 1287–1317
[21] Gatti C, Saunders V R and Roetti C 1994 *J. Chem. Phys.* **101** 10686–10696
[22] Hehre W J, Radom L, von R Schleyer P and Pople J 1986 *Ab initio molecular orbital theory* (New York : John Wiley & Sons) ISBN 978-0-471-81241-8
[23] Smirnov M, Kuznetsov V, Roginskii E, Cornette J, Dutreilh-Colas M, Noguera O, Masson O and Thomas P 2018 *J. Phys.: Condens. Matter* **30** 475403
[24] Vrillet G, Lasbrugnas C, Thomas P, Masson O, Couderc V, Barthélémy A and Champarnaud-Mesjard J C 1988 *J. Phys. C: Solid State Phys.* **21** 4611–4627
[25] Cornette J, Merle-Méjean T, Mirgorodsky A, Colas M, Smirnov M, Masson O and Thomas P 2010 *J. Raman Spectrosc.* **42** 758–764
[26] Ahmed M A K, Fjellvåg H and Kjekshus A 2000 *J. Chem. Soc., Dalton Trans.* 4542–4549
[27] Lindqvist O, Mark W and Moret J 1975 *Acta Crystallogr., Sect. B: Struct. Crystallogr. Cryst. Chem.* **31** 1255–1259
[28] Lindqvist O and Moret J 1973 *Acta Crystallogr., Sect. B: Struct. Crystallogr. Cryst. Chem.* **29** 643–650
[29] Jain H and Nowick A S 1981 *Phys. Status Solidi A* **67** 701–707
[30] Wang C C 1970 *Phys. Rev. B: Condens. Matter Mater. Phys.* **2** 2045–2048
[31] Adler S L 1962 *Physical Review* **126** 413–420
[32] Wiser N 1963 *Physical Review* **129** 62–69
[33] Okada M, Takizawa K and Ieiri S 1977 *J. Appl. Phys.* **48** 4163–4167
[34] Duclère J R, Hayakawa T, Roginskii E M, Smirnov M B, Mirgorodsky A, Couderc V, Masson O, Colas M, Noguera O, Rodriguez V and Thomas P 2018 *J. Appl. Phys.* **123** 183105